

See discussions, stats, and author profiles for this publication at: <https://www.researchgate.net/publication/236784253>

Structural Aspects of Lipid Monolayers: Computer Simulation Analyses

ARTICLE *in* LANGMUIR · MARCH 2010

Impact Factor: 4.46 · DOI: 10.1021/la904734b

CITATIONS

5

READS

32

5 AUTHORS, INCLUDING:



Philip Shushkov

University of Bonn

9 PUBLICATIONS 55 CITATIONS

[SEE PROFILE](#)



Maria Velinova

Sofia University "St. Kliment Ohridski"

9 PUBLICATIONS 55 CITATIONS

[SEE PROFILE](#)



A. Tadjer

Sofia University "St. Kliment Ohridski"

66 PUBLICATIONS 431 CITATIONS

[SEE PROFILE](#)

Structural Aspects of Lipid Monolayers: Computer Simulation Analyses

Philip Shushkov,^{†,‡} Stanislav Tzvetanov,[†] Maria Velinova,[†] Anela Ivanova,[†] and Alia Tadjer^{*,†}

[†]Laboratory of Quantum and Computational Chemistry, Department of Physical Chemistry, Faculty of Chemistry, University of Sofia, 1 James Bourchier Avenue, 1164 Sofia, Bulgaria, and [‡]Department of Chemistry, Yale University, 225 Prospect Street, New Haven, Connecticut 06520-8107

Received December 16, 2009. Revised Manuscript Received February 2, 2010

Extensive molecular dynamics simulations at room temperature were carried out for model films of two dissimilar lipids (DPPC and dicaprin) at the air/water interface. To study the peculiarities of the organization patterns at different average areas per molecule, surface concentrations corresponding to five almost equally spaced points along the isotherms of the two surfactants were considered. A variable of prime interest was the density distribution in a direction normal to the interface of the monolayer components: interfacial water and surfactant on one hand and the separate moieties of the lipids on the other hand. The packing pattern and cluster size dispersion were studied by means of Voronoi tessellation and radial distribution functions. Speculations regarding structural changes upon phase-state changes during film compression were made. Individual characteristics for surfactant heads and tails as well as for interfacial water were outlined and related to the available experimental data. An analysis of the diffusion coefficients revealed the limiting factors for lipid lateral and normal diffusion. Structural arguments in support of changes in monolayer dielectric properties with the area per molecule were provided.

Introduction

Insoluble monolayers spread at the air/water interface have multiple applications both as suitable model systems for a variety of physicochemical, spectroscopic, and microscopic studies and as precursors of Langmuir–Blodgett films.^{1–3} Lipids are a class of amphiphiles used very often as the constituent surfactants of Langmuir monolayers.⁴ Among them, dipalmitoylphosphatidylcholine (DPPC) is probably the most popular nonionogenic surfactant used for this purpose.

Knowledge about the structure and organization of lipid monolayers in general and of those formed by DPPC in particular is of prime importance in several fields of science. Pure or mixed lipid monolayers are employed as models of cell membranes because they are suitable targets of a number of experiments aimed at unveiling the mechanism of transport through cell membranes.

Structural information about monolayers can be supplied by various experimental methods^{1–3,5–17} or extracted from molecular simulations on monolayers or bilayers. The latter procedures are more often coarse-grained^{18–21} because this approach allows investigations of larger systems at a lower computational price. However, the united-atom techniques obscure the detailed picture provided by all-atom estimations; therefore, the latter are preferred in a number of cases.

The latest progress in experimental studies on DPPC monolayers and multilayers that sheds light on their structure and organization^{3,6,7,9,10,12–14,16,17} focuses on the application of various microscopy and spectroscopy techniques. Here we report communication directly related to the simulations in this article. Using CD spectroscopy, AFM measurements, and Laurdan fluorescence, the effects of temperature and pressure on the lateral organization of model membranes are assessed.⁶ The advantages of time-resolved grazing incidence X-ray scattering out of the specular plane versus conventional X-ray specular reflectivity are convincingly presented and used for the study of equilibrium and nonequilibrium states of monolayers at liquid surfaces.⁷ GISAXS studies on DPPC monolayers on pure water reveal the layer thickness and electron densities. Images of DPPC-enriched bilayers obtained using fluorescence optical microscopy⁹ have been subject to Voronoi analysis of the closest neighbors to show that the nucleation rate is proportional to the number of neighbors. Image inspection also discloses that domains positioned closer together are smaller than domains situated far from each other,

*Corresponding author. E-mail: tadjer@chem.uni-sofia.bg. Tel: +35928161374. Fax: +35929625438.

(1) Gaines, G. L., Jr. *Insoluble Monolayers at Liquid-Gas Interfaces*; Wiley-Interscience: New York, 1969.

(2) (a) Moehwald, H. *Annu. Rev. Phys. Chem.* **1990**, *41*, 441. (b) Moehwald, H. In *Handbook of Biological Physics*; Lipowsky, R., Sackmann, E., Eds.; Elsevier: Amsterdam, 1995; Vol. 1, Chapter 4.

(3) Lucero, A.; Rodriguez Nino, M. R.; Gunning, A. P.; Morris, V. J.; Wilde, P. J.; Rodriguez Patino, J. M. *J. Phys. Chem. B* **2008**, *112*, 7651–7661.

(4) *Physical Chemistry of Biological Interfaces*; Baszkin, A., Norde, W., Eds.; Marcel Dekker: New York, 2000.

(5) Kaznessis, Y.; Kim, S.; Larson, R. *Biophys. J.* **2002**, *82*, 1731–1742.

(6) Periasamy, N.; Teichert, H.; Weise, K.; Vogel, R. F.; Winter, R. *Biochim. Biophys. Acta* **2009**, *1788*, 390–401.

(7) Wiegart, L.; O'Flaherty, S. M.; Terech, P. *Langmuir* **2009**, *25*, 4104–4110.

(8) Jing, H. Y.; Hong, D. H.; Kwak, B. D.; Choi, D. J.; Shin, K.; Yu, C.-J.; Kim, J. W.; Noh, D. Y.; Seo, Y. S. *Langmuir* **2009**, *25*, 4198–4202.

(9) Bernchou, U.; Ipsen, J. H.; Simonsen, A. C. *J. Phys. Chem. B* **2009**, *113*, 7170–7177.

(10) Mao, G.; Desai, J.; Flach, C. R.; Mendelsohn, R. *Langmuir* **2008**, *24*, 2025–2034.

(11) Aida, T.; Yamamoto, T.; Ou-Yang, W.; Manaka, T.; Iwamoto, M. *Jpn. J. Appl. Phys.* **2008**, *47*, 411–415.

(12) Ou-yang, W.; Yamamoto, T.; Aida, T.; Manaka, T.; Iwamoto, M. *Thin Solid Films* **2008**, *516*, 2649–2651.

(13) Rodriguez Nino, M. R.; Lucero, A.; Rodriguez Patino, J. M. *Colloids Surf., A* **2008**, *320*, 260–270.

(14) Beno, J.; Weis, M.; Dobrocka, E.; Hasko, D. *Appl. Surf. Sci.* **2008**, *254*, 6370–6375.

(15) Klauda, J. B.; Venable, R. M.; MacKerell, A. D.; Pastor, R. W. *Comput. Model. Membr. Bilayers* **2008**, *60*, 1–48.

(16) Livancic, P. W.; Dunn, R. C. *Langmuir* **2008**, *24*, 14066–14073.

(17) Tomoia-Cotisel, M.; Mocanu, A. *Rev. Chim.* **2008**, *59*, 1230–1233.

(18) Gkeka, P.; Sarkisov, L. *J. Phys. Chem. B* **2009**, *113*, 6–8.

(19) Bennett, W. F. D.; MacCallum, J. L.; Tieleman, D. P. *J. Am. Chem. Soc.* **2009**, *131*, 1972–1978.

(20) Poghosyan, A. H.; Shahinyan, A. A. *Comput. Phys. Commun.* **2009**, *180*, 238–240.

(21) Duncan, S. L.; Larson, R. G. *Biophys. J.* **2008**, *94*, 2965–2986.

which means that at higher surface concentration the domains should remain smaller. Continuously varying surface pressure combined with IR intensity is informative with respect to multilayer formation in a mixed monolayer of lung surfactant.¹⁰ Structure, elasticity, topography, and film thickness by means of surface pressure (Π)–area (A) isotherms combined with BAM and AFM reveal the structural polymorphism of DPPC monolayers at different surface pressures³ and around the collapse point.¹³ The maximum height of the pure DPPC monolayer is assessed from AFM measurements through spontaneously arising holes demonstrating heterogeneity even for the tightest packing.¹⁷ Pure and mixed DPPC monolayers, investigated by Π/A isotherms, X-ray reflectivity, and AFM, provide information about the orientational structure of monolayers.¹⁴ On the basis of $\Pi-A$ isotherm analysis, the creation of stable structures with hexatic ordering is explained. The monolayer thickness (X-ray) and roughness (AFM) are estimated. The application of single-molecule fluorescence (SMF) is presented in a spectacular way by Livanec and Dunn.¹⁶ Invoking the mildest perturbation of the system, SMF affords studies of molecule orientation with separate assessments of the head and tail tilts.

Recent contributions^{15,18–20,22–24} present highlights of the structural studies of lipid films of DPPC by means of molecular simulations. Part of them aim at the validation and extension of molecular force field parameter sets.¹⁵ New GROMACS parameters coming from the simulated WAXS halo shapes, peak maxima, and fwhm²⁰ are used in all-atom and united-atom simulations, proving that the all-atom concept should be favored above the united-atom one in molecular dynamics simulations because the atomistic approach gives results that are closer to measured data than those of united-atom models. An improvement of CHARMM by the introduction of a new charge set for DPPC is suggested and tested by Taylor et al.²³ Although focused on the particular problem of the water isotope effect on lipid bilayer properties, the study by Rog et al.²² provides abundant isotope-free results that can be used as a reference for comparison with monolayer simulations, such as the layer thickness, tail order parameters, lifetime of trans–gauche occurrence, C–C, P–P, and P–N, and H-bond radial distribution functions (RDFs). The role of water as a bridging, anchoring, and caging medium is pointed out. Important structural information on monolayers includes the study of Duncan and Larson, obtained by employing both the coarse-grained and all-atom approach.²¹ Head tilt angles, RDFs, and pore formation at various temperatures and surface pressures/concentrations are assessed and discussed with respect to the system size and timescale. A large number of points along the Π/A isotherm in the LE/LC region of pure and mixed DPPC films are simulated by Rose et al.²⁴ Results from GROMACS electron density plots are used for the tail order parameter and P-P/P-N RDFs. On the basis of the density plots, implications for tail flips are found. In addition to simulations with classical force fields, quantum mechanical calculations on DPPC and kindred lipids^{25,26} augment the structural information related to the conformations of heads and tails known to date.

(22) Rog, T.; Murzyn, K.; Milhaud, J.; Karttunen, M.; Pasenkiewicz-Gierula, M. *J. Phys. Chem. B* **2009**, *113*, 2378–2387.

(23) Taylor, J.; Whiteford, N. E.; Bradley, G.; Watson, G. W. *Biochim. Biophys. Acta* **2009**, *1788*, 638–649.

(24) Rose, D.; Rendell, J.; Lee, D.; Nag, K.; Booth, V. *Biophys. Chem.* **2008**, *138*, 67–77.

(25) Yin, J.; Zhao, Y.-P. *J. Colloid Interface Sci.* **2009**, *329*, 410–415.

(26) (a) Krishnamurti, S.; Stefanov, M.; Mineva, T.; Begu, S.; Devoisselle, J. M.; Goursot, A.; Zhu, R.; Salahub, D. R. *ChemPhysChem* **2008**, *9*, 2321. (b) Krishnamurti, S.; Stefanov, M.; Mineva, T.; Begu, S.; Devoisselle, J. M.; Goursot, A.; Zhu, R.; Salahub, D. R. *J. Phys. Chem. B* **2008**, *112*, 13433.

Simple fatty lipids such as dicaprin (DC) attract much less attention compared to phospholipids. Their application is mostly for the investigation of enzymatic hydrolysis kinetics,^{27,28} and they have hardly ever been a target of intricate molecular modeling. However, it is interesting to compare the properties of such surfactants with DPPC to find out whether some general lipid features could be formulated.

The available structural information extracted from MD simulations of lipid monolayers is limited and fragmentary. Usually they refer to a specific surface concentration, and thus the structural changes upon compression cannot be inspected. Typically, mainly density plots, radial distribution functions (RDFs), and tail order parameters are presented. The purpose of this article is to simulate the behavior of DPPC and DC films in the LE/LC/SC region of the isotherms and to monitor the structural changes that they undergo upon compression. The information contained in the mass and number density plots is discussed in detail, and integral parameters of the monolayer are formulated. The polymorphism of the system is demonstrated by an exhaustive analysis of the Voronoi polygons, including space and time correlation functions. To our knowledge, such a combined approach has not been used so far. The data obtained together with RDFs and order parameters are rationalized in terms of monolayer organization patterns and the size and lifetime of domains at different surface concentrations. Similarities and dissimilarities in the two kinds of lipid films are outlined. The size effect and simulation length are discussed. The structural transformations upon film compression allow a comprehensive interpretation of another set of properties closely related to monolayer structural parameters, namely, the electric and dielectric characteristics of the same systems, which are addressed in a companion article.²⁹ We believe that the results reported in the two articles augment the knowledge of insoluble lipid monolayers at the air–water interface.

Models and Computational Protocol

This section outlines the construction of models and the computational scheme used. Models with 25 and 81 lipids were built under 3D periodic boundary conditions, as specified in our previous studies,^{30,31} in order to test the effect of the elementary cell (EC) size on the computational results. A hexagonal lattice and explicit water molecules were used throughout (Figure 1).

A detailed computational protocol is provided as Supporting Information (Figures S1 and S2 and Tables S1–S3) as well as in the companion article.²⁹ In brief, 10 ns MD simulations in an *NVT* ensemble were carried out for model monolayers at the vacuum/water interface with surface concentrations from 40 to 80 Å²/molecule (DPPC) and from 50 to 80 Å²/molecule (DC) using the explicit TIP3P water model. (TIP4P in one case is a model for the water molecules.)

GROMACS 3.3.3, VMD 1.8.6,³² and original scripts were used for the construction of the EC, batch calculations, vector

(27) (a) Nannelli, F.; Puggelli, M.; Gabrielli, G. *Mater. Sci. Eng., C* **1999**, *445*–450. (b) Ziomek, E.; Douchet, I.; Ivanova, M.; Verger, R. *Chem. Phys. Lipids* **1996**, *81*, 1–9. (c) Rao, C. S.; Damodaran, S. *Langmuir* **2002**, *18*, 6294–6306.

(28) (a) Cajal, Y.; Busquets, M. A.; Carvajal, H.; Girona, V.; Alsina, M. A. *J. Mol. Catal. B* **2003**, *22*, 315–328. (b) Rogalska, E.; Ransac, S.; Verger, R. *J. Biol. Chem.* **1993**, *268*, 792–794. (c) Gargouri, Y.; Pitroni, G.; Riviere, C.; Sardat, L.; Verger, R. *Biochemistry* **1986**, *25*, 1733–1738.

(29) Tzvetanov, S.; Shushkov, P.; Velinova, M.; Ivanova, A.; Tadjer, A. *Langmuir* **2010**, *26*, doi: 10.1021/la9047352.

(30) Shushkov, P. G.; Tzvetanov, S. A.; Ivanova, A. N.; Tadjer, A. V. *Langmuir* **2008**, *24*, 4615–4624.

(31) Tadjer, A.; Ivanova, A.; Velkov, Y.; Tzvetanov, S.; Gotsev, M.; Radoev, B. *Int. J. Quantum Chem.* **2007**, *107*, 1719–1735.

(32) Humphrey, W.; Dalke, A.; Schulten, K. *J. Mol. Graphics* **1996**, *14*, 33–38.

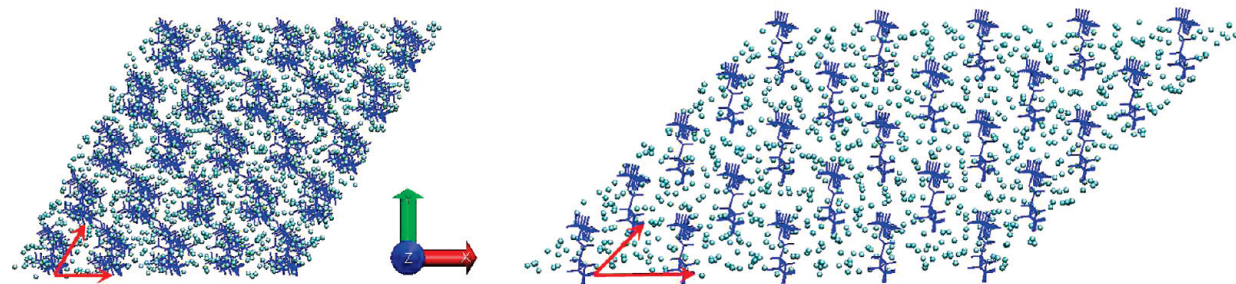


Figure 1. Top view of a monolayer of elementary cells containing 25 DPPC molecules at $50 \text{ \AA}^2/\text{molecule}$ (left) and 25 DC molecules at $60 \text{ \AA}^2/\text{molecule}$ (right). Unit translation vectors and the orientation of the Cartesian coordinate system are also shown.

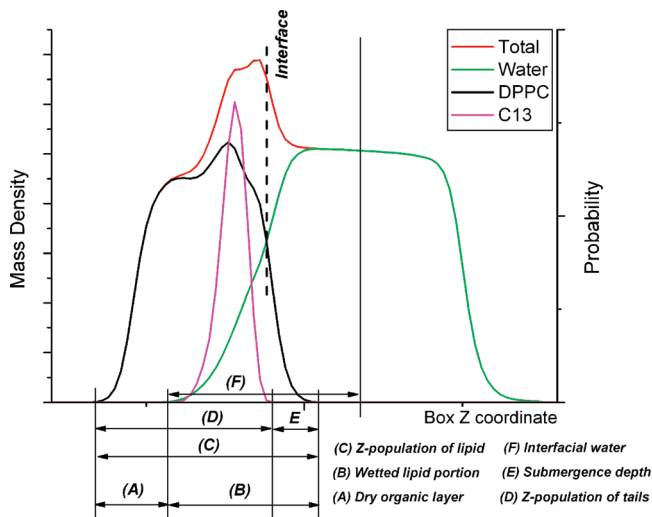


Figure 2. Schematic representation of the parameters derived from density distribution plots.

decomposition, visualization, and statistical analysis of the results. Snapshots were extracted from the trajectory for analysis at intervals of 1 ps, with the entire analyzed ensembles consisting of 10 000 structures. All mean values shown below were averaged over the whole set, and the statistical accuracy was quantified by the standard error.

Results and Discussion

Density Distribution. The mass density distribution in the system can supply valuable structural information. Several general parameters of the monolayers can be extracted upon inspection of the mass and particle density profiles (Figure 2). Part of these are collected in Tables 1 and 2. We have assumed all values of mass density greater than 10^{-4} g/cm^3 and number density greater than 10^{-4} to be significant. Another notion that needs to be specified for a detailed discussion of the plots is the position of the interface. A reasonable assumption is to define the interface as the plane normal to the *z* coordinate at the intersection of water and lipid mass density profiles as done by other authors.²²

Plots of the mass density distributions of the monolayers (modeled with the largest clusters), together with the number density profiles of characteristic atoms of the two lipids, are presented in Figure 3. The following atoms were selected as characteristic: phosphorus (P1) and nitrogen (N8) from the choline group of DPPC and oxygen (O1) from the free hydroxyl group of DC. The density distributions of the branching carbon atoms (C13 of DPPC and C3 of DC) were also analyzed. The plots for the smaller systems are provided as Supporting Information

(Figures S3 and S4). The profiles are based on data from the last 10 ns of the 81- and 25-lipid systems and the last 5 ns of the 9-lipid ones. Although the 9-lipid models were treated with a different protocol, the data are included for comparison.

The thickness of the monolayer has been an issue of ubiquitous speculation based on fragmentary experimental data or modeling.^{3,7,14} It is questionable whether the normal dimensions of the monolayer should be estimated only with respect to the volume populated by surfactant molecules or whether it should include the hydration shells as well. We have made separate measurements of the lipid and water components.

First we have determined the *z* population of the lipid. It spans different portions of the normal to the interface direction (hereafter referred to as the normal direction and normal components of the parameters of interest) depending on the level of compression and the size of the model. For both lipids at any cluster size, the *z* population has identical behavior: an almost constant value at low compression with a sizable increase in the region of high surface concentration. In the case of DPPC models, this increase is more pronounced, amounting to ca. 40% for 81DPPC and to 30% for 9DPPC in the $70\text{--}40 \text{ \AA}^2/\text{molecule}$ interval. For DC, this increase is milder: for the area interval of $80\text{--}50 \text{ \AA}^2/\text{molecule}$, it ranges from less than 20% for 81DC to less than 10% for 9DC. It is worth emphasizing that the lipid *z*-population width grows with the cluster size, which may be due to a combination of reasons rooted in the size effect: enhanced mobility in the normal direction, an opportunity for the formation of multilayer structures, and so forth. However, the estimate of $44 \pm 1 \text{ \AA}$ at $40 \text{ \AA}^2/\text{molecule}$ is in very good agreement with AFM measurements of DPPC layers.¹⁷ There, the headgroup-tail and tail-atmosphere interface roughness values are found to increase during compression.

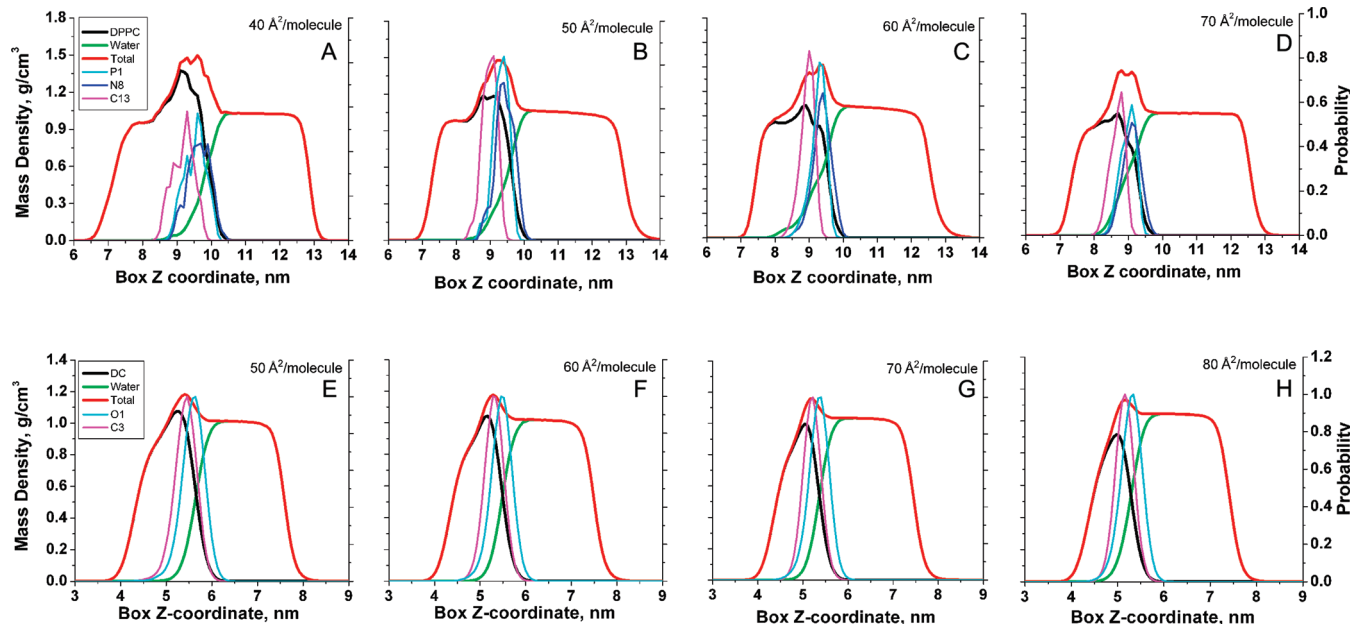
To interpret these dissimilar data, we have partitioned the total lipid *z* population in several ways. The submergence depth of the lipids was estimated to be the lipid population beyond the interface plane. As seen from the results in Tables 1 and 2, this parameter varies within a very narrow range upon compression. It decreases slightly in the case of DPPC and is practically constant for DC. The size effect is also insignificant for both lipids. However, the portion of the lipids “seeing” water (lipid and water density above 10^{-4} g/cm^3), called the wetted lipid portion, exceeds two to three times the submergence depth. This parameter is more markedly size-sensitive and changes in a nonidentical manner for the two lipids. In the case of DPPC, it has a minimum at $60 \text{ \AA}^2/\text{molecule}$, and in the DC models, it grows steadily with compression. The wetted portion of the lipid never exceeds the fully extended length (32.3 \AA) of the DPPC molecule obtained from quantum mechanical calculations,³¹ which means that none of the molecules are squeezed out in the water medium upon compression. In contrast, for 81DC this parameter has higher values than

Table 1. Structural Parameters Extracted from the Mass Density Profiles of DPPC Films (Figures 3, 4, and S2-3)

area, Å ² /molecule	40			50			60			70			80		100		120
no. of DPPC	9	25	81	9	25	81	9	25	81	9	25	81	9	25	9	9	9
z population of DPPC, Å	37.0	39	44	35.5	37	37	30.5	32	36	28.5	33	31	30.5	32	29.5	29.5	
wetted lipid portion, Å	15.5	17.5	25	19.5	21	22	16.5	18	26	17	22	22	17	24	19	20	
z population of tails, Å	29	28	38	29.5	25	31	23.5	25	29	21	25	26	24	25	23	24	
submergence depth, Å	5.0	7.0	8.0	5.0	7.0	7.0	5.0	6.0	9.0	7.0	7.0	7.0	9.0	9.0	9.0	11	
dry organic layer thickness, Å	21.5	21.5	19.0	16.5	16.0	15.0	14.0	16.0	10.0	11.5	11.0	9.0	13.5	8.0	10.5	9.5	

Table 2. Structural Parameters Extracted from the Mass Density Profiles of DC Films (Figures 3 and S2-3)

area, Å ² /molecule	40				50				60				70				80		100		120
no. of DC	9	9	25	81	9	25	81	9	25	81	9	25	81	9	25	81	9	9	9	9	9
z population of DC, Å	25.5	24.0	27.0	29.5	22.0	24.0	27.5	22.5	23.5	25.0	20.5	23.0	25.0	20.0	20.5	20.5	20.5	20.5	20.5	20.5	
wetted lipid portion, Å	10.0	14.0	17.0	18.0	13.5	15.5	18.0	13.0	15.5	16.5	12.5	14.5	16.0	14.0	14.5	14.5	14.5	14.5	14.5	14.5	
z population of tails, Å	23.5	20.0	24.6	27.0	21.5	22.0	24.6	21.5	21.2	23.4	19.0	21.2	24.0	18.5	19.5	19.5	19.5	19.5	19.5	19.5	
submergence depth, Å	4.0	4.0	6.0	7.0	5.0	6.0	7.0	5.0	6.0	7.0	5.0	6.0	7.0	6.0	7.0	6.0	7.0	6.0	7.0	7.0	
dry organic layer thickness, Å	15.5	10.0	10.0	11.5	8.5	8.5	9.0	8.5	8.0	8.5	8.0	8.5	9.0	6.0	9.0	6.0	6.0	6.0	6.0	6.0	

**Figure 3.** Mass density plots of 81 DPPC (A–D) and 81 DC (E–H) with the number density distribution of characteristic atoms.

the fully extended lipid (17.3 \AA)³⁰ at both 60 and $50 \text{ \AA}^2/\text{molecule}$. This might be rationalized in terms of dissolving some DC molecules at higher pressure, but a careful inspection of the trajectories at these surface concentrations reveals that this is not the case. What occurs is rather a conformational change in some molecules, leading to a side-split alignment of the tails, with one of them completely submerged in water and the other one sticking out into the air. Thus, the molecule achieves a rod-shaped form and hence reduces its area. This, however, is a short-living phenomenon on the timescale of less than 100 ps and cannot be a route to permanent area reduction.

The latter effect is confirmed by the data for the z population of tails measured as the difference between the lowest z value for the lipid population and the largest z value for the branching carbon (C13/C3) number density. It may be argued that this is not exactly the tail length because it comprises the hydrophilic ester groups but is an easily monitored parameter because the branching carbon is among the least-fluctuating atoms as verified by Tables 3, 4, S4, and S5. The quantum mechanically calculated maximum lengths of the all-trans tails are 24.0 and 12.1 \AA for DPPC and DC, respectively.³¹ The wetted lipid portion of DPPC

barely exceeds the tail length, which confirms that regardless of the head conformation the DPPC molecules are never entirely enveloped in water. However, the z population of tails is smaller than or on the order of the tail length at lower and moderate compression in 9DPPC and 25DPPC models or gradually increases with pressure for the 81DPPC models. It changes with a jump for the areas of 50 and $40 \text{ \AA}^2/\text{molecule}$, but the largest estimate does not surpass 1.6 times the tail length. This excludes the side-split tail flip and may be due to either (i) anti to gauche transitions followed by dipping of the kinked part in water or (ii) positioning the lipid molecules at different levels with respect to the interface, indicating the formation of a multilevel film or the occurrence of “waves”. The first option would result in an increase in the average area per molecule³³ and should be regarded as less probable at high surface concentration. Rather, the second one is operative as will be confirmed below by other data analysis. In the DC film, the z population of tails retains a constant value for each cluster size until the last stage of compression when it rises by ca. 10%, which falls within the

(33) Shinoda, W.; Okazaki, S. *J. Chem. Phys.* **1998**, *109*, 1517–1521.

Table 3. Particle Density Data for DPPC Models^a

area, Å ² /molecule	40				50				60				70			
	9	25	81	9	25	81	9	25	81	9	25	81	9	25	81	9
no. of DPPC																
d_w at intersection	0.608	0.636	0.636	0.620	0.638	0.638	0.607	0.637	0.609	0.635	0.635	0.635	0.635	0.635	0.635	0.635
z population	6.5	8.0	17.0	8.5	12.0	14.0	7.0	8.0	15.0	8.0	10.0	8.0	10.0	10.0	10.0	14.0
of Cl3, Å																
Cl3 maxima, Å (d_w , g/cm ³)	-7.0(0.126)	91(0.044)	86(0.021)	-7.0(0.139)	85(0.006)	84(0.015)	-5.5(0.337)	89(0.302)	89(0.304)	-11.5(0.020)	83(0.032)	-7.5(0.421)	88(0.403)	88(0.382)	88(0.382)	88(0.382)
d_w																
-5.0(0.078)	94(0.141)	89(0.042)	-4.5(0.216)	88(0.048)	91(0.249)	92(0.243)										
-5.0(0.148)	96(0.148)	93(0.127)	97(0.402)													
ratio of Cl3																
population	1.5:1	2:3:1	1:4:2:	2:7:1	1:5:4:13	1:13										
$fwhm$ Cl3, Å																
z population	4.0 ^b	4.3 ^b	6.9 ^b	2.6 ^b	4.5 ^b	6.1	2.6	2.8	4.9	1.9	3.5	5.0				
of P1, Å	7.0	9.0	17.0	9.0	13.0	15.0	7.5	8.0	17.0	8.0	11.0	11.0				
P1 maxima, Å (d_w , g/cm ³)	-5.0(0.078)	93(0.089)	91(0.059)	-3.5(0.298)	88(0.048)	87(0.055)	-3.0(0.389)	93(0.421)	93(0.563)	-4.5(0.477)	87(0.305)	89(0.459)	89(0.459)	89(0.459)	89(0.459)	89(0.459)
d_w																
-3.0(0.192)	95(0.144)	96(0.3039)	-1.0(0.569)	92(0.243)	94(0.443)	-1.5(0.411)										
-1.5(0.382)	97(0.270)	3(0.127)	95(0.402)													
ratio of P1																
population	1:1.5:1.4	1:3:3.5	1:1.4:2:1	2.8:1	1:10:2:3	1:1:1	1:1	1:1	1:1	1:1	1:1:2	1:1:2	1:1:2	1:1:2	1:1:2	1:1:2
$fwhm$ P1, Å																
z population	5.6 ^b	4.7 ^b	6.8 ^b	3.3 ^b	4.0 ^b	5.8 ^b	3.4 ^b	3.0	5.0	2.3	3.9 ^b	5.8				
of N8, Å	10.5	11.0	19.0	10.5	15.0	18.0	10.0	10.0	20.0	10.5	14.0	14.0				
N8 maxima, Å (d_w , g/cm ³)	-5.5(0.064)	96(0.148)	91(0.059)	-4.5(0.216)	91(0.179)	89(0.135)	-2.5(0.396)	93(0.421)	93(0.563)	-7.5(0.421)	87(0.305)	91(0.593)	91(0.593)	91(0.593)	91(0.593)	91(0.593)
d_w																
-3.5(0.175)	99(0.560)	95(0.242)	-3.5(0.298)	96(0.452)	94(0.443)	-0.5(0.566)										
-2.0(0.411)	97(0.403)	-0.5(0.632)	2(0.911)	100(0.955)	97(0.773)	1.0(0.899)										
-0.5(0.447)	99(0.632)															
1.0(0.694)																
2.5(0.957)																
ratio of N8																
population	3.6:5.7:6.9:	2:1	1:2:7:	2.6:5:9:	1:4:5:1	1:5:3:5	2.9:1:6:1									
$fwhm$ N8, Å																
head tilt, degrees	4.2:4.7:1	2.7:2.7	4.4:1	8.7 ^b	4.9 ^b	4.7 ^b	6.6 ^b	3.4 ^b	5.0	6.5	3.5 ^b	4.6				
	6.8 ^b	5.2	36.4 ÷ 101.1	78.9 ± 5.6	90.0 ± 6.5	78.9 ± 5.6	90.0 ± 6.5	90.0 ± 6.5	90.0 ± 6.5	90.0 ± 6.5	84.5 ± 5.4	78.9 ± 5.6				
	(54.8) ^c	(54.8)	(0.0 ÷ 101.1)	(54.8)	(39.7)	(54.8)	(39.7)	(39.7)	(39.7)	(39.7)	(54.8)	(54.8)	(54.8)	(54.8)	(54.8)	(54.8)

^a Error margins: 9DPPC – 0.5 Å; 25DPPC and 8IDPPC – 1.0 Å. ^b Formal fwhm of a multipeaked profile. ^c Numbers in parentheses denote a second possible orientation.

Table 4. Particle Density Data for DC Models^a

area, Å ² /molecule	50			60			70			80		
no. of DC	9	25	81	9	25	81	9	25	81	9	25	81
<i>d</i> _w at intersection	0.501	0.546	0.543	0.530	0.541	0.536	0.533	0.537	0.536	0.527	0.539	0.531
<i>z</i> population of C3, Å	8.0	14.7	19.4	11.5	14.4	17.4	13.5	13.4	16.0	11.0	14.0	15.8
C3 maxima, Å (<i>d</i> _w , g/cm ³)	1.0 (0.133)	54.6 (0.200)	54.6 (0.237)	6.5 (0.002)	52.8 (0.161)	52.8 (0.197)	7.5 (0.003)	52.2 (0.227)	52.2 (0.281)	2.5 (0.243)	51.6 (0.257)	51.6 (0.321)
ratio of C3 population				1.5 (0.241)			2.0 (0.281)					
ratio of O1 population				1:48			1:68					
fwlm C3, Å	2.3	4.6	5.3	3.1	4.4	4.8	3.5	4.2	4.5	3.7	4.1	4.5
<i>z</i> population of O1, Å	9.0	16.3	23.4	14.5	17.0	20.6	14.5	17.8	18.8	12.5	18.0	18.6
O1 maxima, Å (<i>d</i> _w , X ³)	0.5 (0.520)	55.8 (0.400)	56.4 (0.520)	6.5 (0.002)	55.2 (0.595)	54.6 (0.483)	0.5 (0.553)	54.0 (0.565)	54.0 (0.602)	0.5 (0.628)	53.4 (0.593)	53.4 (0.626)
ratio of O1 population				0.0 (0.544)								
fwlm O1, Å	2.9	4.8	5.5	3.4	4.6	5.2	3.8	4.4	5.0	3.7	4.5	5.2

^a Error margins: 9DC – 0.5 Å; 25DC and 81DC – 0.6 Å.

margin of error. At all surface concentrations and model sizes, however, the value of this parameter is more or less twice as large as the maximum tail length, which is evidence that side-split flips occur at any level of compression. The effect is obviously size-sensitive and most pronounced in the largest models.

Subtraction of the wetted lipid portion from the *z* population of lipids makes possible the assessment of the dry organic layer thickness (i.e., the thickness of the lipid layer void of water). In DPPC models, this parameter doubles its value upon compression by a gradual nonlinear increase. In DC films, the thickness retains a constant value until the last stage of compression when it grows less markedly than DPPC. The thickness of dry DC may be assumed to be roughly 10 Å irrespective of the surface concentration whereas for DPPC it varies approximately from 10 to 20 Å upon decrease in the average area per molecule. Such estimates might be of interest with respect to the surfactant contamination of water reservoirs where vital characteristics (e.g., optical properties and gas exchange) depend on the thickness of the organic layer. The results compare well with estimates by other authors.^{22,23}

Another set of useful data could be extracted from the number density distribution plotted in Figure 3 and collected in Tables 3, 4, S4, and S5.

The stages of compression from LE to LC regions of DPPC are predominantly accompanied by the reorganization of the heads in terms of hydration, individual orientation, and mutual alignment. On the basis of the number density distribution of three characteristic atoms—the branching carbon (C13), phosphorus (P1), and nitrogen (N8)—a general scenario of compression effects can be outlined. At 70 Å²/molecule, all three characteristic atoms are sufficiently hydrated. C13 and N8 have comparatively narrower *z* populations and P1 spans a larger portion of the normal direction. However, N8 and P1 have almost identical fwhm values that are larger than that for C13. Judging by the P1 data, part of the lipids (about 40%) tend to stay closer to the interface, ca. 2 Å higher than the remaining surfactants. The main peaks of P1 and N8 are very close, indicating an orientation of the P–N vector, which is predominantly parallel to the interface. The profiles of the P1 and N8 distributions are shifted with respect to each other, indicating an overall lower position of N8 than P1. The quantum mechanical assessment of the P–N distance is 5.2 Å.³¹ A similar value can be obtained upon extrapolation of the data in ref 25 to full hydration. The ratio of the distance between the peaks of the profiles of P1 and N8 to this reference distance provides information about the prevailing angle of the P–N vector with respect to the normal

direction. The estimates of this parameter, named the head tilt, are presented in Table 3, and the calculated values agree nicely with experimental evaluations.¹⁶ In most models, however, a second, less populated value of the head tilt appears, giving preference to a more stretched lipid conformation. In the cases of multipeaked distributions, the different combinations of peak pairs can yield a variety of head tilts. At 70 Å²/molecule, the head tilt resulting from the population data is in the range of 78.9 ± 5.7° to 90.0 ± 6.5°, also depending on the cluster size.

At 60 Å²/molecule, the distributions (*z* population) of C13 and P1 remain the same whereas that for N8 broadens markedly and becomes more asymmetric, especially in the 81DPPC models. This implies a variety of alignments and orientations of the P–N vector. For 81DPPC, the peaks reveal that a majority of the heads are well hydrated but some molecules fall into the range of depleted water. The positions of the maxima show that the predominant head tilt for 81DPPC and 25DPPC is 90°, and the smallest models again suggest a more extended conformation. The large dispersion of the number density and the horizontal P–N orientation can be rationalized as enhanced disorder at this surface concentration, which could be attributed to the coexistence of several types of organization as is further elaborated on below. No signs of multilevel formation are visible for the larger models, whereas in 9DPPC there are distinct tokens of stratification.

The next two stages of compression feature number density profiles with complex structure. They clearly indicate the superposition of several distributions, already distinguishable at 50 Å²/molecule and well recognizable at 40 Å²/molecule. Two lipid levels could be identified in 81DPPC at 50 Å²/molecule on the basis of the synchronous shift in the C13, P1, and N8 maxima: ca. 10% of the molecules form an upper, scarcely hydrated level, with the remaining lipids residing in the aqueous medium. Two orientations of the P–N vector can be specified for the latter group: parallel to the interface and forming an angle of ~55° with respect to the normal direction.

The stratification is even more notable in 25DPPC, where three levels can be discriminated and the head tilt varies from about 40 to >80°. Livanec and Dunn have reported very similar results when observing DPPC monolayers with fluorescence microscopy.¹⁶ At the same surface concentration (ca. 50 Å²/molecule), they have also registered two different head-tilt angles for the lipids. For those heads lying in the plane of the monolayer, amounting to 39%, they have obtained tilts >81°, in excellent agreement with our data. The remaining lipids have shown either

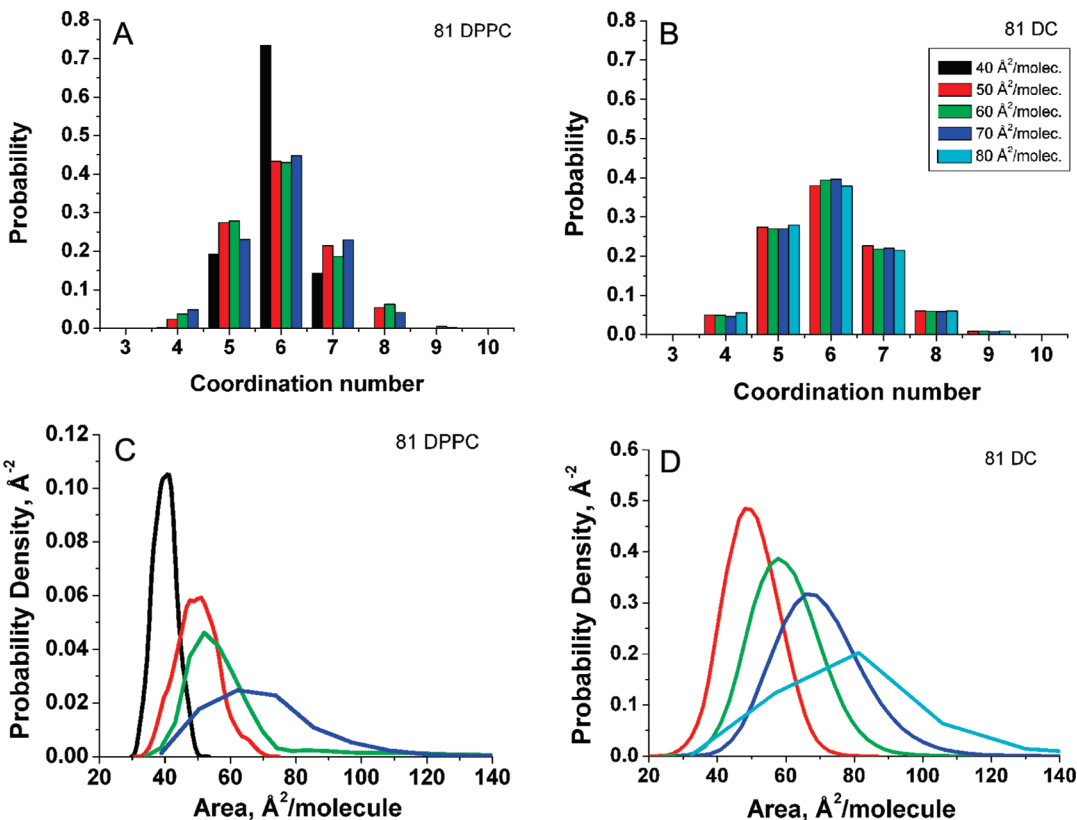


Figure 4. Coordination number (A, B) and area distribution (C, D) of DPPC (A, C) and DC (B, D) monolayers with 81 lipids in the EC at different surface concentrations. In all cases, the standard errors are an order of magnitude lower than the respective average values.

small head tilts of <10° (42%) or all other possible orientations (19%). When considering the last two groups together, one comes up with an average value that is very close to our estimate of ca. 50°.

The closest packing at 40 Å²/molecule features the most pronounced stratification. The distribution of each characteristic atom is quite broad for every model, and several subdistributions are easily discernible. Four levels could be outlined in 81DPPC and three in the smaller models. A majority of the heads belong to the middle level(s), and the uppermost and lowest levels are less populated. Correspondingly, the uppermost level is almost dehydrated at each cluster size and only the lowest is beneath the interface. Because 40 Å²/molecule is close to the point of collapse of the DPPC film, this structural information signifies that compression does not cause the dissolution but rather the accumulation of lipid molecules. Hypothetically (because of the multitude of peak pairs), the head tilt may vary over a very broad interval. However, if we consider the sublevels separately, the value would be closer to 90 ± 6.5°, which makes the average cross section of the molecule quite large. Hence, stratification facilitates tight packing. The formation of a multilevel DPPC monolayer permits the more favorable electrostatic interaction of the zwitterionic heads and could be expected in other amphiphiles with markedly polar heads.

As a general observation, it can be noted that the *z* population and the fwhm of the monitored atoms vary with the size of the cluster, being smallest for the 9DPPC and largest for the 81DPPC models at any surface concentration; the 25DPPC clusters behave like the small models at 40 and 60 Å²/molecule and are more like the large models at 50 and 70 Å²/molecule. Another aspect of the size effect is that the monitored parameters in the smaller models lag behind those in the large one (e.g., the specific behavior of

81DPPC at 60 Å²/molecule is typical for smaller models at 70 Å²/molecule).

Water is depleted in a nonlinear manner in a certain direction with respect to the lipid tails in most cases. In all models, there is a water density tail protruding up to a certain tail carbon, typically the second or third carbon of the tail of the lowest-level lipids at low compression and of the middle-level lipids at high compression.

In contrast to the complex shapes of the density and the probability profiles in DPPC models, the respective plots for DC are perfectly uniform. The *z* distributions and fwhm of the two characteristic atoms—branching carbon C3 and the oxygen from nonesterified OH group O1—grow monotonously with compression irrespective of the cluster size. Their *z* populations at the highest surface concentration definitely exceed the full length of the molecule, implying the sinking rather than the accumulating pattern of collapse. Regardless of the model size, the C3 and O1 peaks are always displaced by 2 Å and the fwhm differs by 0.2 Å. Both atoms are sufficiently hydrated at any degree of compression, with O1 in all plots being deeper in water than C3. Notwithstanding the population width, no distinct indication of multilevel organization is witnessed at any surface concentration. However, because of the broad population, surface roughness is also to be expected. The head tilt cannot be defined because of the nonspecific head structure. Water depletion in a certain direction with respect to the tails has a linear trendline ending with a shoulder typically protruding to the fourth carbon of the tails.

Overall, the maximum lipid mass density grows with compression and is of the same order of magnitude for DC and unilevel DPPC films (1 ± 0.1 g/cm³). Both lipids reach their maximum density above the interface plane. The water share with respect to mass

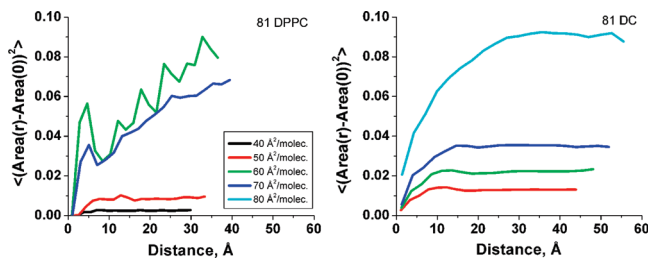


Figure 5. Area-area space correlation function vs the distance between the lipid centers of mass of DPPC (left) and DC (right) monolayers with 81 lipids in the EC at different degrees of compression.

density at the water-lipid intersection also grows insignificantly with compression, being ca. 0.640 and 0.540 g/cm³ for DPPC and DC, respectively.

Voronoi Analysis. Voronoi analysis³³ was performed for the systems with 81 lipids in the elementary cell in order to determine the type of packing in the two monolayers in terms of the number of nearest neighbors and the areas of the polygons formed by them around a given lipid. The latter can be interpreted as the region occupied by a lipid molecule in the monolayer or as the instantaneous area per lipid. In line with the initially imposed hexagonal lattice and with the fact that the MD simulations were carried out in an *NVT* ensemble, an average value of 6 for the coordination number is anticipated whereas the mean area should coincide with the initial area per molecule of the particular system. Figure 4 summarizes the neighbors and the area distributions of the DPPC and DC monolayers.

The results in Figure 4 confirm the expected behavior: six-coordinate lipids are indeed the most populated at all areas per molecule and the area distributions have their maxima at the respective initial area per molecule. Apart from that, relatively broad ranges of coordination numbers and areas are registered. The number of nearest neighbors for both lipids can range from four to nine. The minimum area occupied by a DPPC molecule is ca. 30 Å²/molecule, and for DC, this value is about 20 Å²/molecule. This is a reasonable difference, keeping in mind the bulkier head of DPPC. The maximum areas depend on the surface concentration and reach up to 115 Å²/molecule for DPPC at 70 Å²/molecule and up to 200 Å²/molecule for DC at 80 Å²/molecule. Both the nearest neighbors and the areas are characterized by Gaussian distributions around the average value. However, some of the shapes are rather distorted. Five- and seven-coordinate lipids have substantial shares in the two monolayers at all points along the isotherm, with the slight predominance of the smaller coordination number. The overall share of five- and seven-coordinate molecules varies for DPPC between 31% at 40 Å²/molecule and 46% at 60 and 70 Å²/molecule, going through a maximum of 49% at 50 Å²/molecule. These fractions are larger than the ones obtained by other authors on the basis of shorter trajectories.³³ The respective value for DC is constant (49%) for all areas. This is an indication of the existence of a significant fraction of more irregularly packed lipids in the two films, which deviate from the strict hexagonal arrangement. The only exception is DPPC at 40 Å²/molecule, where an expressed preference for hexagonal packing exists, as verified by the high peak of coordination number 6 at the expense of the strongly reduced fraction of the rest of the coordination numbers. This signifies the solid-state-like packing of DPPC at this point. Such exact ordering is not achieved at any area in the DC monolayers, where the shares of the various coordination numbers vary immaterially along the entire isotherm.

Table 5. Correlation Lengths (r_{corr} , Å) and Typical Domain Diameters ($d = 2r_{corr}$, Å) of DPPC and DC Monolayers at Different Degrees of Compression (Å²/Molecule) Estimated from the Area-Area Space Correlation Functions (Figure 5)

area	81 DPPC		81 DC		d
	r_{corr}	d	area	r_{corr}	
40	14	28	50	13	26
50	12	24	60	14	28
60	> 40		70	24	48
70	> 40		80	37	74

The tight packing of DPPC at 40 Å²/molecule is corroborated by the very narrow and practically undistorted Gaussian of the area distribution. The curves in the three larger areas, however, are characterized by asymmetric tails extending toward the large areas. These tails are evidence of the existence of a second, less ordered phase at milder monolayer compression. Well-discernible curve tails and plateaus on the Gaussians are not observed for DC monolayers in the range of 50–70 Å²/molecule. These degrees of compression are described by almost symmetric and relatively broad Gaussian area distributions, becoming broader at lower surface concentrations. This illustrates the decreased degree of lipid ordering and the increased mobility (see also the discussion of diffusion coefficients in the Supporting Information) of this lipid compared to DPPC. Whatever structural rearrangements take place in the DC films, they are gradual and exclude a marked coexistence of two distinctly different phases.

The monolayers of the two lipids have very wide ranging area distributions (Figure 4) at the lowest surface concentrations studied (70 Å²/molecule for DPPC and 80 Å²/molecule for DC), where small and large areas are almost equally populated. This reflects the existence of more tightly packed lipid domains separated by neat water regions, or “pores”, which is in conjunction with the location of these points along the isotherms, namely, in the region where the LC and LE states coexist. The presence of ordered lipid substructures even at such small degrees of compression is interesting, with the latter being confirmed by the radial distribution functions. (See the next section.) This fact is often disputed when attempts to interpret the experimental data are made.¹

The characteristic size of the lipid domains formed at a given degree of compression can be extracted from the area-area space correlation functions³⁴ of the two monolayers, which are presented in Figure 5. The individual polygon areas obtained from the Voronoi analysis were used.

When the correlation in the area fluctuations decays, the space correlation function (SCF) should reach a plateau. The value where the SCF levels off is the characteristic distance at which the lipid molecule areas become uncorrelated (i.e., the correlation length). It can be interpreted as a typical radius of the lipid domains formed at the respective degree of compression.

The data in Figure 5 show a relatively strong dependence of the calculated area-area SCFs on the surface concentration. Whereas the curves of the DPPC monolayer at 40 and 50 Å²/molecule saturate quite fast, the SCFs at the two lower degrees of compression show much more enhanced correlation between the areas and practically do not reach constant values within the studied ECs. The area-area correlation in the DC films grows more gradually with the decrease in the degree of compression. In this case, only the areas at 80 Å²/molecule are significantly more

(34) Allen, M. P.; Tildesley, D. J. *Computer Simulation of Liquids*; Oxford University Press: Oxford, U.K., 2002.

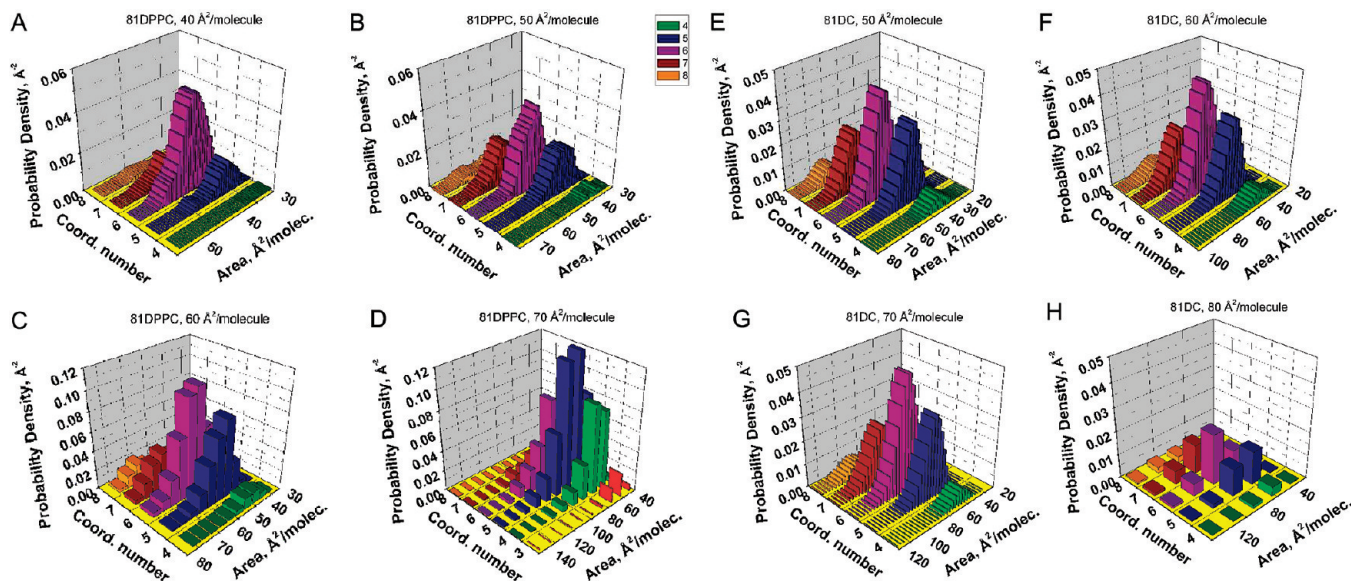


Figure 6. Double histograms combining the distributions of areas and coordination numbers obtained from the Voronoi analysis of DPPC (A–D) and DC (E–H) monolayers with 81 lipids in the elementary cell at different degrees of compression.

correlated than those at the other points. However, a plateau is achieved even for this surface concentration within the simulated distance range, which is an indication that the chosen size of the lipid elementary cells is sufficient for most of the concentrations studied. The EC might need to be extended only for DPPC for areas larger than $50 \text{ Å}^2/\text{molecule}$.

The correlation lengths of the studied systems were obtained after fitting the SCFs to an exponential or power law growth curve, and their values are collected in Table 5.

The characteristic domain sizes of DPPC and DC monolayers at high compression are similar and vary slightly at around 25 Å even though the two lipids are quite different in structure and electrostatic behavior. This is a convincing example of universal behavior, which actually is to be expected by general arguments, namely, symmetry considerations. (See the nearest-neighbor distributions.) Thus, the size of the domains does not seem to be the determining factor in the collapse of the film because such a small domain size is reached by the two monolayers at different areas per molecule and the systems continue to fluctuate around it until the collapse. At lower degrees of compression, the typical domain size grows appreciably by almost doubling in value at every $10 \text{ Å}^2/\text{molecule}$ step for DC whereas for DPPC the dimension even extends beyond the available elementary cell. The increased size of DC domains with short-range order over the larger areas per lipid is in line with the trends in the radial distribution functions (see the next section) and indicates the existence of lipid ordering even in the state that is experimentally interpreted as liquid-expanded and is traditionally believed to be of a disordered nature.¹ In summary, unlike the traditional notion of the homogeneous 2D LE phase, the film is a very heterogeneous admixture of somewhat ordered irregularly shaped domains and neat water pores. In fact, this is not a novel observation, but what we have attempted to show is how the structural picture arises and changes along the isotherm.

The time correlation functions (TCFs)³⁴ of the individual lipid areas yielded by the Voronoi analysis provide a different type of information, which is summarized in the Supporting Information. They can be used to extract characteristic area–time correlation lengths (τ_c), which can be interpreted as the mean time of domain existence, and to test the sensitivity of τ_c to the degree of

compression of the monolayers. The TCFs for DPPC and DC with 81 lipids in the elementary cell are presented in Figure S5, and the correlation times are summarized in Table S6.

The coordination number and area distributions obtained from the Voronoi analysis are combined into the double histograms shown in Figure 6. With decreasing compression, the peaks of the two films become sharper and taller, with the highest one always corresponding to six-coordinate molecules at the respective area per molecule. As could be expected, the smallest and largest numbers of neighbors, as well as areas, are the least populated. At the same time, those small populations can be used as markers of the structural rearrangements taking place upon compression of the monolayers. The two most expanded DPPC layers are characterized at all coordination numbers by very long tails protruding to areas well beyond $200 \text{ Å}^2/\text{molecule}$, which correspond to the share of disordered lipids. These tails are more populated at $60 \text{ Å}^2/\text{molecule}$, which confirms the reorganization of the monolayer at this degree of compression. The two higher surface concentrations of the monolayer demonstrate very interesting behavior. The various coordination numbers are described by more or less distinct bimodal area distributions. At $50 \text{ Å}^2/\text{molecule}$, lipids with four and five neighbors have the highest maxima of their distributions around $40 \text{ Å}^2/\text{molecule}$ and those with seven and eight neighbors also appreciably populate the areas around $60 \text{ Å}^2/\text{molecule}$. Obviously, these two regions overlap for the six-coordinate lipids to give a broad distorted Gaussian. The overall distribution clearly reveals the coexistence of two types of packing (a tighter and a looser one) in the DPPC monolayer at this surface concentration. At $40 \text{ Å}^2/\text{molecule}$, the two types of packing are preserved but the share of the more loosely bound lipids decreases substantially. This may be related to the multipeaked density distributions or to the broad head tilt range. All DC double histograms consist of single Gaussian peaks. This shows that there is no coexistence of various types of ordering at any degree of layer compression. The maxima of the distributions shift gradually to larger areas with an increasing number of nearest neighbors varying always within $\pm 10 \text{ Å}^2/\text{molecule}$ with respect to the corresponding mean area per molecule. In line with the smaller lateral sizes of DC compared to DPPC, the large-area tails extend to lesser areas in the DC

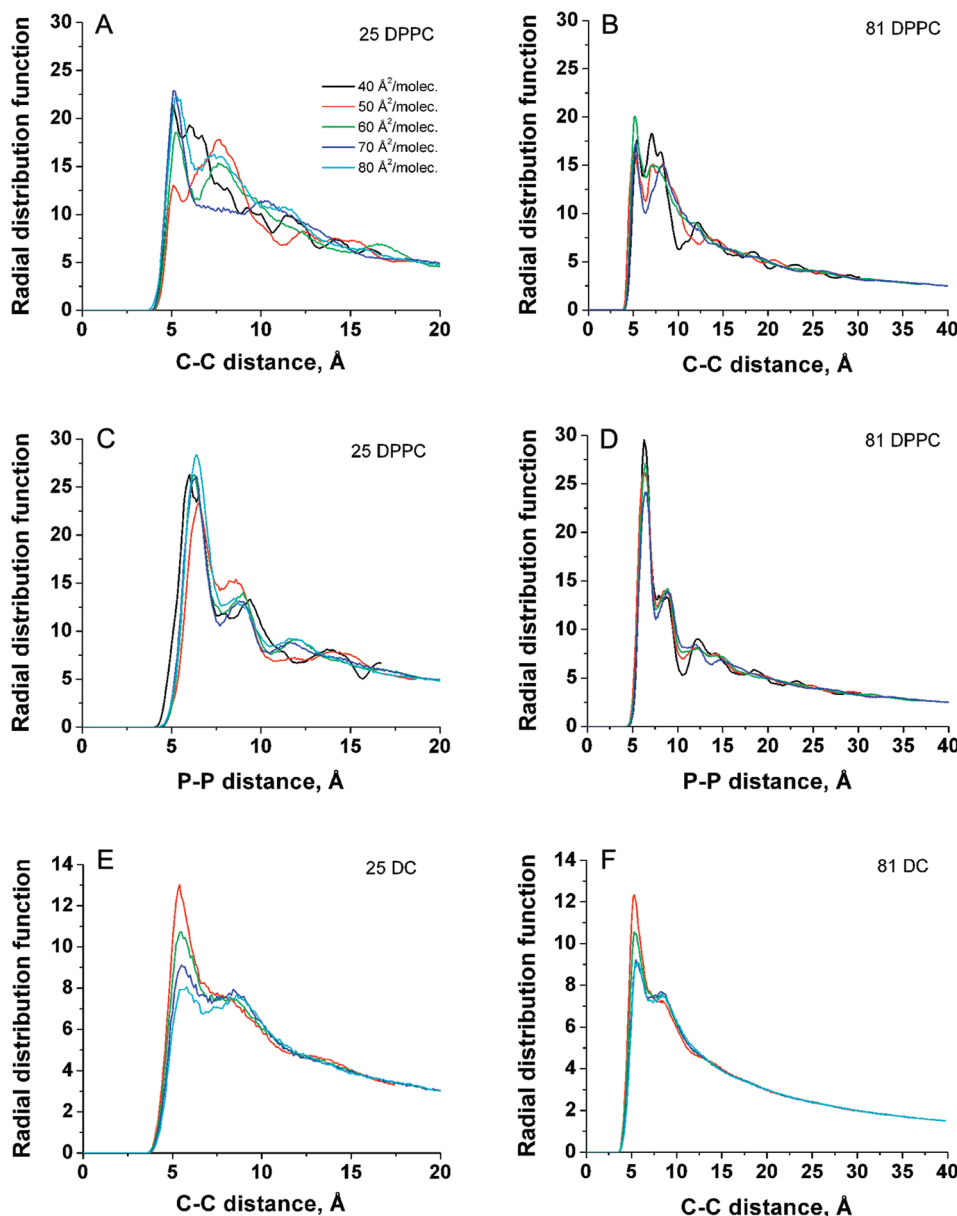


Figure 7. Radial distribution functions of DPPC (A–D) and DC (E, F) monolayers with 25 (A, C, E) and 81 (B, D, F) lipids in the elementary cell at different degrees of compression.

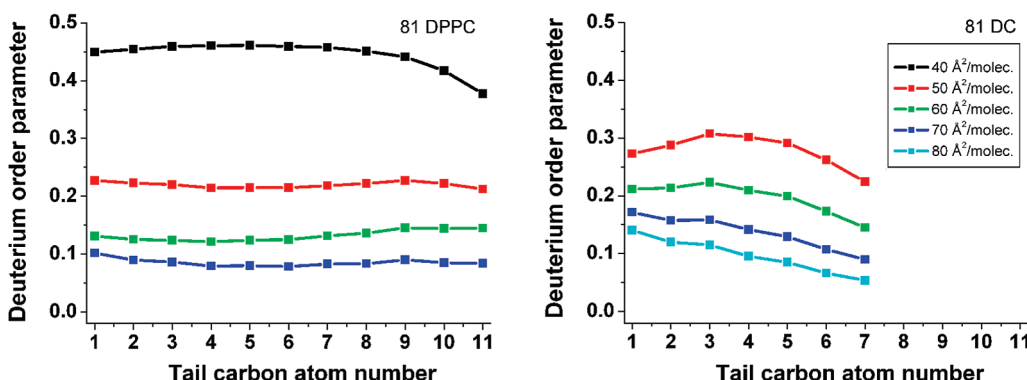


Figure 8. Deuterium order parameters of the hydrocarbon tails for DPPC (left) and DC (right) films modeled with 81 lipids. Average data for the two tails. Carbon atoms are numbered from the third atom after the branching site toward the tail end.

monolayers with the exception of the point at the lowest surface concentration. Nevertheless, there are still well-shaped maxima of

five-, six-, and seven-coordinate lipids over relatively small areas. This means that the DC monolayers at this mild compression

preserve some ordered structures separated by large water pores. From the various large areas that are populated we can assume that there are lipids between the domains that are free to occupy a broad range of areas (i.e., they are highly disordered at this surface concentration). Similar comments are valid for DPPC at 60 Å²/molecule. In the latter case, however, the percentage of the ordered lipids is much more prominent (notice the different probability axis scaling). Moreover, the packing is markedly more centered at the six-coordinate organization.

Radial Distribution Functions. More information about the type of packing in the studied monolayers can be extracted from the radial distribution functions (RDFs). The branching carbon atoms of the two lipids were used to calculate the pair distribution functions because they are the most rigid sites of the molecules and can thus be considered to be structure-representative. In addition, the phosphorus–phosphorus RDFs were analyzed for DPPC because the P atoms monitor the ordering of the DPPC heads. The respective RDFs are shown in Figure 7.

All carbon–carbon radial distribution functions (Figure 7) for the models with 81 lipids show a very sharp first peak at 5.3 Å (DPPC) or 5.5 Å (DC) followed by a second peak with lower intensity at 8.2 Å (DPPC) or 8.4 Å (DC). This is the fingerprint of a liquid (or amorphous solid) type of ordering in the two monolayers, which is analogous in spite of the substantially different molecular structure of the two lipids. This agrees with the similarity of the minimum characteristic domain sizes (Table 5) predicted from the Voronoi analysis. It is interesting that the distance between the carbons corresponding to the first peak is even smaller than the initial lipid separation at the highest surface concentration, which means that the molecules have formed more closely packed structures during the MD simulation. The accommodation of the nearest neighbors at such small distances can be explained by the substantial displacement of the lipids in the z direction, as witnessed from the density distributions. (See above.)

The ratio between the distances of the second and first maxima is ~1.55 for DPPC and ~1.53 for DC. These numbers are larger than the theoretical values of a square lattice and smaller than those of a hexagonal one. Thus, both lipids maintain significantly distorted hexagonal, or the so-called hexatic, alignment at all surface concentrations. In fact, the two peaks correspond to two types of first neighbors around a given lipid, forming a distorted hexagon as its immediate surrounding. The liquid type of packing is more feasible for DC because there are no further distinctive peaks in the RDFs indicating solidlike long-range order. It is noteworthy that the intensity of the second peak of the DC films gradually decreases from 70 to 50 Å²/molecule, which indicates a decrease in lipid hexagon distortion when the surface pressure grows. The second peak almost disappears at 50 Å²/molecule where a very mild third maximum at a distance of around 13 Å is observed. However, the overall shape of the latter curves resembles liquid-type behavior of the lipids. On the contrary, the packing in the DPPC films is solidlike because of the appearance of well-shaped, albeit weak, maxima (up to six at 40 Å²/molecule) at larger distances both in the C–C and in the P–P RDFs. The monolayer reorganization at 60 Å²/molecule is supported by the shape of the second maximum, which has a very broad plateau ranging from 7.0 to 7.7 Å.

Apart from the two main peaks discussed, the DPPC carbon–carbon RDFs have an additional specific feature—a well-shaped intermediate peak at 7.2 Å appears only at the two highest degrees of compression. It relates to the first peak as ~1.4. This implies the presence of a second type of squarelike packing in the DPPC films at these surface concentrations, which is in accordance with the

structural rearrangements implied by the Voronoi analysis (Figure 6). At 50 Å²/molecule, the distorted hexagonal arrangement is predominant whereas at 40 Å²/molecule the two types of packing are almost equally populated with the new one slightly prevailing. An alternative hypothesis would be that the additional peak stems from lipids, which are forced to occupy intermediate separations in the distorted hexagons because of the substantial external pressure.

The number of peaks is preserved in the phosphorus–phosphorus RDFs of DPPC, which also confirms the presence of long-range ordering for the surfactant heads. However, the positions of the two main maxima are shifted to larger distances—6.4 Å for the first one and 8.8 Å for the second one—in accordance with the bulkier zwitterionic surfactant head. The ratio between the two peaks decreases to ca. 1.4, which means that the DPPC heads are arranged in a tighter square lattice, unlike the hexatic ordering of the tails. The intermediate maximum appears at 7.9 Å in the P–P curves as well but only at the highest degree of compression. This suggests more regular ordering of the heads where the formation of a new arrangement is possible only at very high surface pressure.

Even though the smaller models containing 25 lipids in the elementary cell have less accurate statistics per se, their radial distribution functions preserve all of the main features discussed above. The distances to the maxima do not vary by more than 0.4 Å. Thus, the type of organization discussed above is present in the monolayers modeled by the smaller clusters.

Order Parameters. The tail order parameters³⁵ of the two lipids (Figures 8 and S6) provide additional support of the above-stated hypotheses.

In DPPC models, the order parameter seems to grow continuously with compression.

In 81DPPC (Figure 8), the order parameter grows more steadily with compression from 70 to 50 Å²/molecule, with all atoms having almost identical values. A slight deviation can be registered at 70 and 50 Å²/molecule in the atoms closest to the head with a somewhat higher magnitude and in the farthest ones with the lowest ordering. In contrast, the tail termini are most ordered at 60 Å²/molecule, an indication of essential structural changes occurring at this surface concentration, as confirmed by the Voronoi analysis and RDFs. (See above.) Since this point in the isotherm corresponds to the range of coexistence of phases, the formation of unilayer condensed domains results in enhanced hydrophobic interactions reflected in improved ordering of hydrocarbon chains. The curve at 40 Å²/molecule reveals two peculiarities: (i) the values are twice as high as compared to 50 Å²/molecule and (ii) the carbons in the middle of the chain are more ordered than the ones farthest from the head. The atom closest to the head has a slightly lower value that may originate from two factors: either this is the atom where the trans–gauche transition occurs, or, more probably, close packing invokes a variety of head alignments, which results in partial disorder of the adjacent tail carbons. Again, because of the dense packing, only the end-of-chain atoms can afford some freedom. In particular, if a multilevel structure is formed, the chain-end atoms of the top-level lipids would have sufficient space for enhanced motion. Qualitatively, the results reproduce the experimental profiles very well as measured from the NMR spectra³⁶ of bilayers. Quantitatively, our results indicate a higher order, but most

(35) (a) Hubbell, W. L.; McConnell, H. M. *J. Am. Chem. Soc.* **1971**, *93*, 314–326.
(b) Heller, H.; Schaefer, M.; Schulten, K. *J. Phys. Chem.* **1993**, *97*, 8343–8360.

(36) (a) Seelig, A.; Seelig, J. *Biochemistry* **1977**, *16*, 45–50. (b) Seelig, A.; Seelig, J. *Q. Rev. Biophys.* **1980**, *13*, 19–61. (c) Davis, J. H.; Bloom, M.; Butler, K. W.; Smith, I. C. P. *Biochim. Biophys. Acta* **1980**, *597*, 477–491.

probably this is rooted in the lower temperature maintained during the simulation. Apart from some dissimilarities in the profile shapes and grouping, the size effect in the DPPC models is expressed in the overall higher values for 81DPPC at the respective surface concentration with the exception of the curves at 50 Å²/molecule.

In the case of DC (Figures 8 and S6), the values along the tail follow a linear dependence at 80 Å²/molecule, being highest for the head end and lowest for the tail end of the chain. With increasing compression, although the overall order increases, the profiles gradually change their shape, featuring a lower order for the first two carbons closest to the head, which is in line with the observation of a side-split tail flip, followed by a more ordered middle part and ending with the low order of the tail ends. Although the profiles of the two lipids differ in shape for surface concentrations of 80–50 Å²/molecule, the values for DPPC and DC are in the same range: 0.05–0.25. At the highest compression, however, the DPPC tails are much more ordered than those of DC. Comparison of the order parameters for 25-lipid models (Figure S6) shows that the results for DC are completely size-insensitive whereas those for DPPC change both in profile and magnitude depending on the cluster size. An expected result is that in both lipids compression solidifies the middle part of the chains because it is relatively independent of the head mobility and the tail termini thermal fluctuations.

Another type of information about the dynamics of the monolayers can be extracted from the calculated diffusion coefficients (Table S7, Figure S7)

Conclusions

Molecular dynamics simulations of dipalmitoylphosphatidylcholine (DPPC) and dicaprin (DC) monolayers at the gas/water interface were carried out. The systems were modeled with elementary cells of 9, 25, or 81 lipids with hydrophilic parts surrounded by explicit water molecules. All calculations were performed in the *NVT* ensemble at 300 K with periodic boundary conditions applied. The main focus of the study was the determination of key structural parameters of the monolayers and the elucidation of the factors governing lipid organization at the interface. Several surface concentrations along the surface pressure/area isotherms were modeled.

The mass density profiles across the monolayers showed stratification of the DPPC films into several sublayers at the highest degree of compression, but there was no evidence of the formation of multilayered structures of DC. The hydrophilic heads of DPPC turned out to be significantly tilted (average head tilt ca. 90°) with respect to the monolayer normal at all surface concentrations. No indication of the submergence of DPPC or DC molecules into the water subphase at high pressure was witnessed. Instead, stratification (in the case of DPPC) or tail flip (for DC) took place in order to accommodate the adjacent lipids. The water portion included in the monolayers participated actively in the formulation of the film structure.

At all surface concentrations, even at the highest degree of compression, the monolayers of both lipids were characterized by the presence of a substantial fraction of disordered lipids. Broad distributions of the individual lipid areas obtained from Voronoi analysis were observed in the regions with low surface

concentration or where lipid reorganization (DPPC) took place. Abrupt changes in DPPC arrangement upon compression were registered while the DC molecules rearranged smoothly.

It was found that ordered lipid structures existed in both films even at very low surface concentrations. The minimum domain sizes were determined and were found to be similar for the two monolayers at high compression. The characteristic times of domain existence were on the order of several nanoseconds for DPPC and below 2 ns for DC. The presence of reorganization phenomena in the DPPC monolayers was confirmed by plateaus in the time correlation functions persistent over more than 1 ns at certain areas per molecule. Low-frequency periodic motion with the same period was observed in all systems studied.

Bimodal neighbor-area distributions at high surface concentration indicated two types of lipid packing in the DPPC monolayer. The calculated atom-pair radial distribution functions (RDFs) revealed distorted hexagonal (i.e., hexatic) packing of the lipids in the two monolayers. The two peaks, which were always present in the RDFs, were attributed to two types of first neighbors forming an irregularly shaped hexagon around a given lipid. Additional peaks in the RDFs of DPPC films at 40 and 50 Å²/molecule signified a solid type of packing at these areas per molecule.

Tail order parameters grew with compression, with the growth being monotonous for DC and discrete for DPPC. The middle section of the tails always remained more ordered whereas the behavior of the tail termini varied with surface concentration.

The estimated diffusion coefficients in directions normal and tangential to the interface showed that DC does not feature normal diffusion. On the contrary, the diffusion of DPPC normal to the interface was faster than that within the monolayer plane. At low surface concentrations, the DC molecules moved faster than the DPPC molecules. The lateral diffusion of both lipids became slower upon compression, reaching comparable magnitude at areas per molecule larger than 70 Å²/molecule.

Overall, the effect of the elementary cell size was less expressed for the DC films than for the DPPC systems. Within the latter, most of the estimated parameters changed to a different degree upon extension of the models.

Acknowledgment. This research was funded by projects DO-2-256/2008 and DO-2-82/2008 of the National Science Fund of Bulgaria. The Alexander von Humboldt Foundation is acknowledged for an equipment grant.

Supporting Information Available: Details of the computational procedure; number density estimates from DPPC and DC monolayers with 9 lipids in the EC; potential energy fluctuations along the production part of the MD trajectories of the studied systems at 60 Å²/molecule; density profiles of the DPPC and DC monolayers with 9 and 25 lipids in the EC; area-area time correlation functions of the monolayers with 81 lipids in the EC; tail order parameters of the models with 25 surfactants; mean square displacement and diffusion coefficients calculated thereof for DPPC and DC in the films with 81 lipids in the EC. This material is available free of charge via the Internet at <http://pubs.acs.org>.